ACS Catalysis

Research Article

pubs.acs.org/acscatalysis

Surface Structures and Electrochemical Activities of PtRu Overlayers on Ir Nanoparticles

Kug-Seung Lee,[†] Yong-Hun Cho,[‡] Tae-Yeol Jeon,[§] Sung Jong Yoo,[†] Hee-Young Park,[§] Jong Hyun Jang,[†] and Yung-Eun Sung*[,§]

[†]Fuel Cell Research Center, Korea Institute of Science and Technology (KIST), Seoul 136-791, Republic of Korea

[‡]School of Advanced Materials Engineering, Kookmin University, Seoul 136-702, Republic of Korea

[§]School of Chemical and Biological Engineering, Seoul National University (SNU), Seoul 151-744, South Korea

Supporting Information

ABSTRACT: PtRu overlayers were deposited on carbon-supported Ir nanoparticles with various Pt:Ru compositions. Structural and electrochemical characterizations were performed using transmission electron microscopy (TEM), X-ray diffraction, high-resolution powder diffraction (HRPD), X-ray photoelectron spectroscopy (XPS), cyclic voltammetry (CV), and CO stripping voltammetry. The PtRu overlayers were selectively deposited on the Ir nanoparticles with good uniformity of distribution. As a result, the PtRu utilization of the present samples was higher than that of PtRu/C. The mass-specific activities for methanol oxidation were also significantly higher. Single-cell performance using the Pt_2Ru_1 overlayer sample as an anode catalyst was slightly higher than that obtained using commercial PtRu/C despite the fact that the PtRu anode loading for Pt_2Ru_1/Ir/C was only 42% of that of PtRu/C.

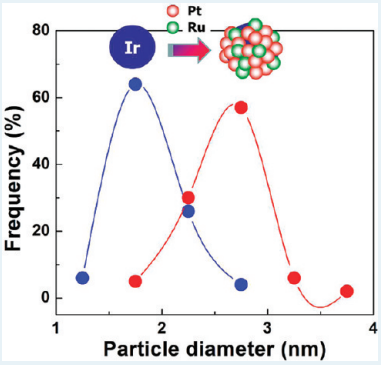

KEYWORDS: *core/shell Structure, PtRu overlayer, Ir nanoparticle, methanol oxidation reaction, surface modification*

1. INTRODUCTION

It has been found that Pt-based electrocatalysts offer good performance when applied to low-temperature fuel cells, including polymer electrolyte membrane fuel cells (PEMFCs) and direct methanol fuel cells (DMFCs). However, the use of Pt makes these fuel cells expensive to produce. Therefore, many attempts have been made to reduce the amount of Pt used in fuel cell electrodes. One method involving the alloying Pt with transition metals has been extensively studied with the objective of enhancing electrocatalytic activity and reducing the Pt content in catalysts. Such alloying methods, however, have not satisfactorily reduced the Pt loading.[1] Reports on the use of non-noble catalysts such as transition metal chalcogenides, oxides, and macrocycles as alternatives to Pt have shown that their electrocatalytic activities are much lower than Pt. The surface modification of metal nanoparticles has been suggested to be a promising candidate for minimizing the amount of Pt used and such modification has been realized by the formation of core/shell structures using chemical,[1−10] electrochemical,[11−15] and surface-segregation methods.[16−18] For DMFCs, the proportion of catalyst costs in the total production cost is much higher than it is in PEMFCs because the amount of catalysts used is greater by approximately one order of magnitude. A low degree of activity and utilization necessitate these high catalyst loadings. Therefore, the formation of core/shell structures for use in DMFCs is highly desirable, an approach that has not been reported much in the literature, except in several papers we have published.[1,7−9,19]

From the practical viewpoint of synthesis, it is necessary to apply chemical syntheses to the formation of core/shell catalysts because other methods, including electrochemical deposition and surface-segregation, are often inappropriate for commercialization. In chemical synthesis methods, a reducing agent can reduce the metal precursors in a solvent, wherein the driving force of the reduction is the difference between the standard potentials of the metal precursors and the reducing agent. To form core/shell structures, it is of vital importance to choose a proper reducing agent in a given synthetic system. If the standard potential of the reducing agent is too low, meaning the difference between standard potentials of the metal (Pt, in this case) precursors and the reducing agent is too large, rapid reduction of Pt can be facilitated, and the reduced Pt atoms can then readily agglomerate to produce independent Pt particles. In addition to the choice of a suitable reducing agent, the surface states of the core particles, including metallic/oxides phases and impurity contents can significantly influence the Pt overlayer structures because of their different surface energies and lattice parameters.[1] To produce highly active core/shell catalysts, the effect of the core material on the intrinsic activity,

Special Issue: Electrocatalysis

Received: December 28, 2011
Revised: February 13, 2012
Published: March 16, 2012

and the effect of size and dispersive state of the core materials have on carbon are also of interest.

We have studied the chemical synthesis of core−shell structured catalysts for direct methanol oxidation using carbon-supported Au and Ir nanoparticles as core particles.[1,7,8,19] Au is a good core material for the uniform deposition of Pt overlayers because it is the noblest metal and, hence, its surface is dominated by the metallic phase. However, the underlying Au negatively affects the electrocatalytic activities of CO and methanol oxidation.[7,8] Ir nanoparticles were therefore adopted as an alternative, and as a result, the deposited Pt overlayer showed a uniform core/shell structure and enhanced mass-specific activity for CO and methanol oxidation.[1] However, the Pt overlayer is not expected to be as active as a PtRu bimetallic overlayer. In this study, PtRu bimetallic overlayers were deposited on carbon-supported Ir nanoparticles with various Pt:Ru ratios to form core/shell structures. Subsequently, the electrocatalytic activity for CO and methanol oxidation and single-cell performance were examined. The activities of the prepared samples were compared with those of a commercial PtRu/C catalyst.

2. EXPERIMENTAL PROCEDURES

2.1. Sample Preparation. To synthesize Ir nanoparticles on carbon (Ir/C), IrO_x nanoparticles were first synthesized on carbon (IrO_x/C) and then the IrO_x/C was reduced to Ir/C. The procedure for synthesizing IrO_x/C and reducing it to form Ir/C is described in detail elsewhere.[1] In brief, a certain amount of Ir precursor ($H_2IrCl_6{\cdot}xH_2O$) was dissolved in an ethylene glycol (EG) solution containing NaOH, followed by refluxing in a three-neck flask at 100 °C for 1 h in an Ar atmosphere and was then left to cool naturally. For the deposition of the IrOx nanoparticles on carbon, a carbon black (Vulcan XC-72R) was dispersed in deionized (DI) water, and then an adequate amount of IrO_x colloid was added to the carbon-dispersed solution and mixed to obtain a mixture with 8 wt % IrO_x/C. After vigorous stirring, 2 M H_2SO_4 was added to the solution to control the solution pH. After additional stirring, the sample was washed and dried. The obtained IrO_x/C was reduced in a tube furnace by flowing 10% H_2/Ar gas to form Ir/C nanoparticles.

The PtRu overlayers were deposited on the Ir/C nanoparticles by adding specific quantities of Pt ($H_2PtCl_6{\cdot}xH_2O$) and Ru ($RuCl_3{\cdot}xH_2O$) precursors to the Ir/C-dispersed anhydrous ethanol (*a*-EtOH) solution. The total volume of the solution was 200 mL. After being stirred for 30 min, adequate quantities of L-ascorbic acid ($C_6H_8O_6$) were introduced to the solution. The solution was stirred for a further 30 min and then heated at 80 °C for 5 h. After cooling to room temperature, the solution was filtered with DI water and evaporated in a vacuum oven. The quantities of Pt and Ru precursors were adjusted to achieve Pt + Ru/Ir atomic ratios of 2, which provided the most active thickness when the Pt overlayers were deposited.[1] The nominal Pt:Ru atomic ratio was controlled to be 3:1, 2:1, and 1:1. Hereafter, the PtRu overlayers on Ir/C samples are designated as Pt_xRu_y/Ir/C, where x and y denote the Pt:Ru ratio. For the purpose of comparison, a commercial catalyst (40 wt % PtRu/C, Etek; referred to as PtRu/C) was also characterized electrochemically.

2.2. Sample Characterization. Transmission electron microscopy (TEM) images were obtained using a JEOL 2010 transmission electron microscope operated at 200 kV. Samples were prepared by placing a drop of catalyst solution onto a carbon-coated copper grid that was subsequently dried. Energy dispersive spectroscopy (EDS) point analysis was carried out using a TEM-EDS system. X-ray diffraction (XRD) analysis was performed using a Rigaku D/MAX 2500 and Cu Kα radiation (λ = 1.541 Å) at 40 kV and 200 mA. The samples were scanned from 20° to 80° (2θ) at a scan rate of 2°/min. X-ray photoelectron spectroscopy (XPS) was performed in a multipurpose surface analysis system (SIGMA PROBE, Thermo, U.K.) operating at base pressures of $<10^{-10}$ mbar. The X-ray source used for this purpose was Al K_α (1486.6 eV) operating at 15 KV and 10 mA. Pt 4f and Ir 4f signals were collected and analyzed by the deconvolution of the spectra using XPS Peak 4.1 software. During the spectra acquisition process, the constant analyzer energy mode was employed with a pass energy of 40 eV at increments of 0.1 eV. The binding energies of the obtained spectra were calibrated using the C 1s peak (284.6 eV). Cyclic voltammetry (CV) was carried out in a conventional three electrode electrochemical cell using a glassy carbon electrode as the working electrode, a Pt wire as the counter electrode, and a saturated calomel electrode as the reference electrode. All electrochemical measurements were reported against the normal hydrogen electrode (NHE). The catalyst inks were prepared by mixing the catalysts, a 5 wt % Nafion solution (Aldrich Chem. Co), and 2-propanol (JUNSEI). The electrochemical experiments were performed using AUTOLAB (Eco Chemie). Prior to taking the measurements, 0.5 M H_2SO_4 and 1 M CH_3OH/0.5 M H_2SO_4 solutions were purged with Ar gas. CO-stripping voltammetry was performed in 0.5 M H_2SO_4 at potentials of 0.05−1.2 V vs. NHE with a scan rate of 20 mV/s at room temperature. CO molecules were attached to the catalysts at a potential of 0.1 V vs. NHE by bubbling the 0.5 M H_2SO_4 solution with 10% CO/He gas for 20 min, after which the dissolved CO gas in the solution was removed by bubbling with Ar gas for 30 min. To determine the activities of the catalysts, CV was performed in 1 M CH_3OH/0.5 M H_2SO_4 at potentials of 0.05−1 V vs NHE at 60 °C at a scan rate of 20 mV/s. Chronoamperometry was measured at room temperature in 1 M CH_3OH/0.5 M H_2SO_4 at 0.5 V.

The catalysts tested were used as anode catalysts, and a commercial Pt black catalyst (Johnson Matthey) was used as the cathode catalyst. To form a fuel cell electrode, catalyst ink was brushed onto a gas diffusion layer (GDL, microporous layer on carbon paper with wet proofing coating, E-TEK). Nafion 115 was used as the membrane, and the anode catalyst loading was 0.5 and 0.35 mg_{metal}/cm^2 for PtRu/C and Pt_xRu_y−Ir respectively. The cathode catalyst loading was 3 mg/cm^2 for both membrane electrode assemblies (MEAs). Polarization curves for each MEA were measured in individual 5-cm^2 cells. To measure the performance of MEA, 1 M methanol solution (1 mL/min) and oxygen (90 mL/min) were fed into the anode and cathode sides, respectively, of the single. The temperature of the single cell was maintained at 60 °C with ambient back pressure.

3. RESULTS AND DISCUSSION

3.1. Structural Characterizations. Ir and Pt_xRu_y/Ir/C nanoparticles were dispersed well on the carbon support, as shown in Figure 1. The Ir nanoparticles were 1−3 nm in size with a mean diameter of 1.92 nm. The particle sizes of the Pt_xRu_y/Ir/C samples were found to be mostly in the range 2−3 nm. The size distribution of the particles (Figure 1e) shows a

dx.doi.org/10.1021/cs2006907 | ACS Catal. 2012, 2, 739−745

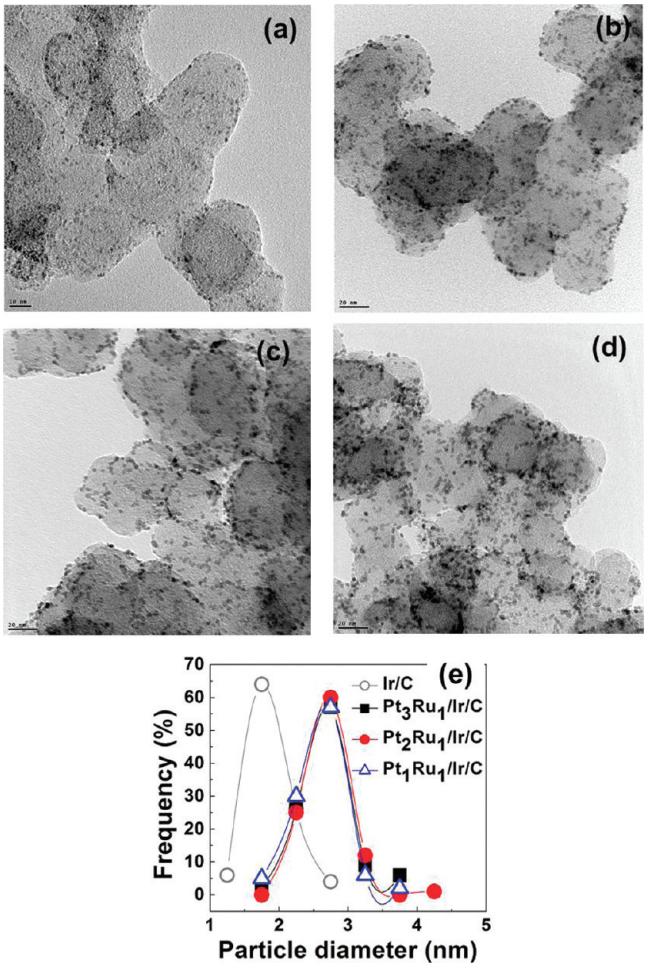

Figure 1. TEM images of (a) Ir/C, (b) Pt_1Ru_1/Ir/C, (c) Pt_2Ru_1/Ir/C, (d) Pt_3Ru_1/Ir/C, and (e) size distribution of prepared nanoparticles supported on carbon.

similar shape of distribution for all the Pt_xRu_y/Ir/C samples. The mean particle diameters were 2.68, 2.76, and 2.81 nm for Pt_1Ru_1/Ir/C, Pt_2Ru_1/Ir/C, and Pt_3Ru_1/Ir/C, respectively, and their theoretical values, as calculated using the following equation were 2.78, 2.79, and 2.8 nm, respectively.[7,20]

$$D_{\mathrm{PtRu/Ir}} = D_{\mathrm{Ir}}\left(1 + [\mathrm{PtRu}]\frac{V_m^{\mathrm{Pt}}\theta_{\mathrm{Pt}} + V_m^{\mathrm{Ru}}\theta_{\mathrm{Ru}}}{V_m^{\mathrm{Ir}}[\mathrm{Ir}]}\right)^{1/3}$$

Here, V_m is the molar volume; [ ] is the atomic ratio between PtRu and Ir (here, [PtRu]/[Ir] = 2); $D_{\mathrm{PtRu/Ir}}$ is the diameter of the Pt_xRu_y/Ir/C nanoparticles; D_{Ir} is the diameter of the carbon-supported Ir nanoparticles; and θ is the atomic fraction between Pt and Ru (for example, $\theta_{\mathrm{Pt}} = 0.75$ and $\theta_{\mathrm{Ru}} = 0.25$ in Pt_3Ru_1/Ir/C). The experimental values correspond closely to the theoretical values within a small range of error. The mean particle diameter of Pt_xRu_y/Ir/C suggests that the thicknesses of the deposited PtRu overlayers correspond to 1.4−1.6 monolayers ($d_{\mathrm{Pt}} = 0.276$ and $d_{\mathrm{Ru}} = 0.268$ nm).[21] These results indicate that the reduced Pt and Ru atoms were deposited selectively on the surface of the carbon-supported Ir nanoparticles. The atomic compositions of individual particles for the Pt_1Ru_1/Ir/C sample were verified using EDS measurement. As shown in Figure 2a, dark-field TEM images were magnified, and a 1 nm-wide spot was focused on individual particles. A representative EDS signal is shown in Figure 2b. The resulting quantification, which is summarized in Table 1, shows that the Pt:Ru:Ir atomic composition is nearly 1:1:1, though it varies from particle to particle. These results indicate that the Pt and Ru quantities were well controlled and that the reduced Pt and Ru atoms were deposited selectively on the surface of the carbon-supported Ir nanoparticles.

XRD profiles of the samples are shown in Figure 3. All the Pt_xRu_y/Ir/C samples showed peak positions that were similar to that of the PtRu/C catalyst. The profiles became broad as the Ru content increased. A Ru-only phase was not detected in all the Pt_xRu_y/Ir/C samples, indicating that Ru was incorporated into the FCC Pt lattice and/or uniformly deposited on Ir and Pt. In our previous paper, the lattice parameter of Pt for a Pt overlayer on an Ir substrate could be obtained by using the whole-pattern profile matching method. However, in the present experiment, profile matching for Pt_xRu_y/Ir/C samples would not be valid because of the complicated crystallographic structure that results from the presence of Ru. The detailed crystallographic structure of the Pt_xRu_y/Ir/C samples requires further and careful investigation.

To analyze the changes in the electronic structure and metallic components along with the compositional changes in the PtRu overlayers, XPS was performed on the Pt_xRu_y/Ir/C samples. Pt 4f, Ru 3p, and Ir 4f signals were collected. The Pt:Ru:Ir ratios were found to be 33.9:36.5:29.6, 46.8:24.1:29.1, and 51.0:17.4:31.6 for the Pt_1Ru_1/Ir/C, Pt_2Ru_1/Ir/C, and Pt_3Ru_1/Ir/C samples, respectively, results that are in good accordance with the synthetic conditions. The signals were deconvoluted into three pairs of doublets, which can be assigned to Pt(0), Pt(II), and Pt(IV) states for Pt;[22] Ru(0), Ru(IV), and Ru(V) states for Ru;[22] and Ir(0) and Ir(IV) states for Ir.[23] The binding energies (BEs) and the atomic composition of each component are listed in Table 2. The deconvolution of the XPS signals is shown in Supporting Information, Figure S1. No shift in BE was detected with changes in the overlayer composition. Upon deposition of the PtRu overlayers, the atomic compositions of the Ir metallic phase increase because the exposed Ir surface area becomes smaller, indicating that the reduced Pt and Ru atoms or clusters are uniformly deposited on the surface of the Ir nanoparticles. This result coincides with the results of the TEM analysis. The atomic compositions of the metallic/oxides phase show no correlation with the changes in the overlayer composition.

3.2. Electrochemical Characterizations and Methanol Oxidation. To characterize the surface of the Pt_xRu_y/Ir/C samples, CV was carried out in 0.5 M H_2SO_4, and the resulting voltammograms are shown in Figure 4a. The Pt_xRu_y/Ir/C samples clearly show different surface characteristics, including H adsorption/desorption (0.05−0.3 V), Pt-oxide formation (0.8 V)/reduction (0.5−0.8 V), and Ru-oxide formation (>0.3 V). As the Pt/Ru ratio decreased, the double-layer capacity increased and the Pt-oxide reduction peak at ∼0.5 V shifted to less positive potentials owing to the oxophilic nature of Ru and the low Ru oxide reduction potential (less than 0.4 V), respectively.[7]

The surface structure was further examined using CO stripping voltammetry, and the results are shown in Figure 4b. The CO stripping peak of the exposed Ir surface was suppressed almost completely, indicating that most of the Ir surfaces were covered with PtRu overlayers. The peak potentials of the Pt_xRu_y/Ir/C samples were found to be more positive than that of PtRu/C. In our previous work,[1] the peak

dx.doi.org/10.1021/cs2006907 | ACS Catal. 2012, 2, 739−745

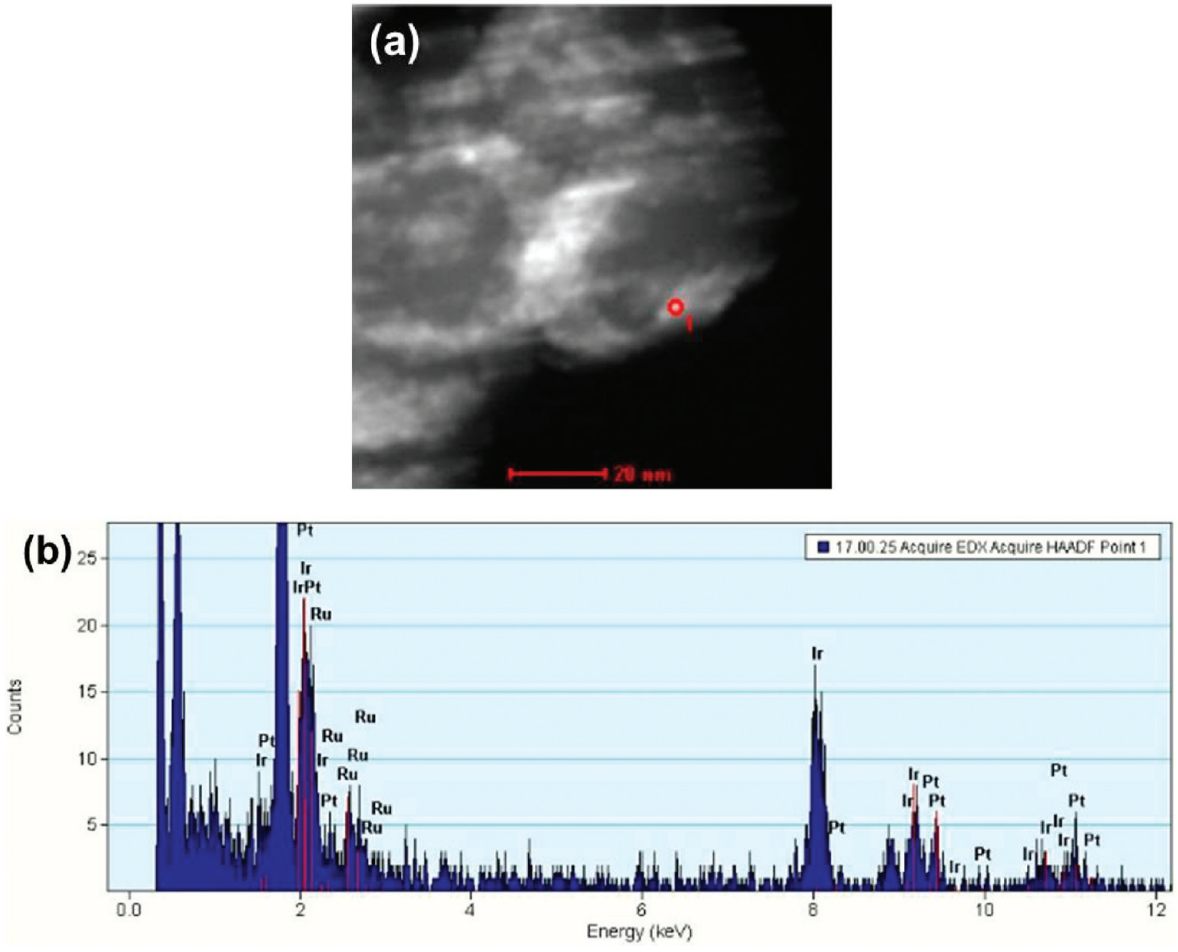

Figure 2. (a) Dark-field TEM image for EDS point analysis (1 nm-wide spot was focused on an individual particle) and (b) representative EDS signal of $Pt_1Ru_1/Ir/C$ sample.

Table 1. Quantification Results of EDS Point Analysis for $Pt_1Ru_1/Ir/C$ Sample

point	Pt (%)	Ru (%)	Ir (%)
1	36.31	31.54	32.15
2	28.62	34.10	37.26
3	23.48	28.01	48.51
4	32.15	33.86	33.99
5	35.24	31.26	33.50
6	34.18	35.60	30.22

potential of the Pt overlayer on Ir nanoparticles was slightly more negative than that of Pt/C when the Pt/Ir atomic ratio equaled 2. In the present experiment, the Pt + Ru/Ir ratio was also controlled to be 2. This suggests that the influence of the underlying Ir on the CO stripping characteristics of the PtRu overlayers differ from that of the Pt overlayer. For the Pt overlayers on the Ir nanoparticles, the negative shift of the CO stripping peak potentials was attributed to a downshift of the Pt d-band on Ir, which could be related to the weakened Pt−CO bonding. For the PtRu overlayers on the Ir nanoparticles, Ru−CO bonding, or the effect of Ru on the Pt-CO bonding might affect the CO_{ad} oxidation activity in such a way as to shift the CO stripping peaks positively. Hammer−Norskov d−band model predicted that the shift of the Ru d-band center of the Ru overlayer on Ir can be positive as compared to that of pure Ru, whereas the shift of the Pt d−band center of the Pt

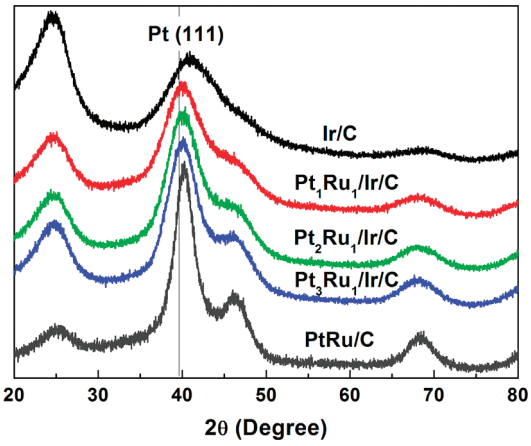

Figure 3. XRD profiles of prepared samples.

overlayer on Ir can be negative as compared to that of pure Pt.[24] Therefore, the Ru−CO bonding of Ru on Ir can be expected to be stronger than that of pure Ru. It should be noted that the CO stripping peaks of the $Pt_xRu_y/Ir/C$ are located at 0.6−0.7 V which is more negative than that of Pt overlayers on Ir (~0.8 V). Therefore, the bifunctional effect due to the addition of Ru on the overlayer is working. The electrochemical surface areas (ESAs) were calculated using CO stripping charges, yielding values of 97.5, 79.3, 71.9, and 59.4

dx.doi.org/10.1021/cs2006907 | ACS Catal. 2012, 2, 739−745

Table 2. Binding Energies of Components and Their Atomic Concentrations in XPS Result

	Pt 4f			Ru $3p_{3/2}$			Ir 4f		
sample	oxidation state	B. E. (eV)	atomic ratio (%)	oxidation state	B. E. (eV)	atomic ratio (%)	oxidation state	B. E. (eV)	atomic ratio (%)
Ir/C							Ir(0)	60.9	44.77
							Ir(IV)	61.98	39.22
								62.5	16.01
Pt_1Ru_1/Ir/C	Pt(0)	71.34	53. 9	Ru(0)	460.86	15.0	Ir(0)	60.88	52.2
	Pt(II)	72.02	27.3	Ru(IV)	462.85	40.9	Ir(IV)	61.67	36.5
	Pt(IV)	73.38	18.8	Ru(V)	465.09	44.1		62.53	11.3
Pt_2Ru_1/Ir/C	Pt(0)	71.24	54.6	Ru(0)	461.26	7.1	Ir(0)	60.84	52.4
	Pt(II)	71.96	28.0	Ru(IV)	463.01	46.3	Ir(IV)	61.51	30.0
	Pt(IV)	73.25	17.4	Ru(V)	465.46	46.6		62.35	17.6
Pt_3Ru_1/Ir/C	Pt(0)	71.23	58.8	Ru(0)	461.00	18.2	Ir(0)	60.87	65.2
	Pt(II)	71.96	24.5	Ru(IV)	462.78	36.8	Ir(IV)	61.75	23.2
	Pt(IV)	73.50	16.7	Ru(V)	465.04	45.0		62.65	11.6

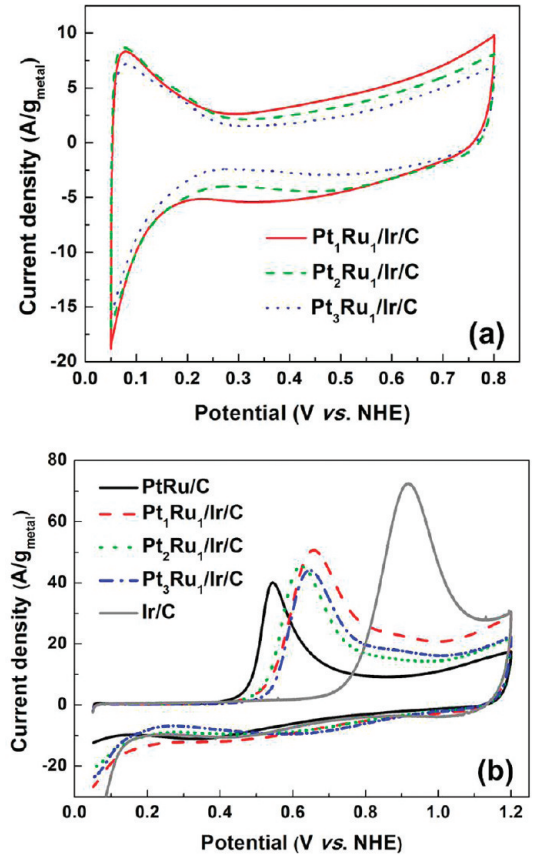

Figure 4. (a) CV and (b) CO stripping voltammetry curves of Ir/C and Pt_xRu_y/Ir/C samples.

m^2/g_{metal} for Pt_1Ru_1/Ir/C, Pt_2Ru_1/Ir/C, Pt_3Ru_1/Ir/C, and PtRu/C, respectively. The ESA of the Pt_xRu_y/Ir/C samples is greater than that of PtRu/C. The ESA decreases gradually as the Pt/Ru ratio increases, indicating better particle dispersion for low Pt/Ru ratios in the synthesis process. Because the surface exposure of Ir was negligible as shown in CO stripping voltammograms, the ESAs can be normalized by PtRu mass, giving values of 150, 118.4, and 102.7 m^2/g_{PtRu} for Pt_1Ru_1/Ir/C, Pt_2Ru_1/Ir/C, and Pt_3Ru_1/Ir/C, respectively. This result suggests that the PtRu utilization of the Pt_xRu_y/Ir/C samples was enhanced over the PtRu/C catalyst by up to ~2.5 times, owing to the formation of the core/shell structure.

Methanol oxidation was performed using CV in 1 M MeOH/0.5 M H_2SO_4 at 60 °C and the oxidation currents were normalized with respect to the total metal or PtRu mass, as shown in Figure 5a and b. The activity order of Pt_xRu_y/Ir/C

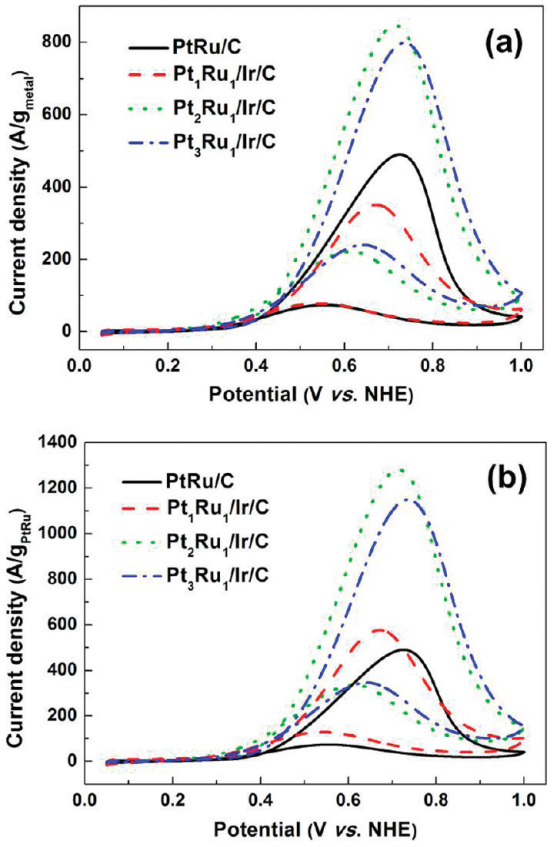

Figure 5. Current densities for methanol oxidation normalized by (a) metal and (b) PtRu masses, which were measured by cyclic voltammetry at 60 °C.

was consistent with the results of CO stripping. This order can result from the competitive contribution of Pt utilization and CO_{ad} oxidation activity. In addition, the underlying Ir might affect the activity of methanol oxidation. Alloy catalysts containing Ir have shown superior methanol oxidation activities relative to PtRu/C catalysts. The improved methanol oxidation activity of the alloy catalysts has been attributed to an enhanced C−H bond activation in the presence of Ir.[25−27] In the present

dx.doi.org/10.1021/cs2006907 | ACS Catal. 2012, 2, 739−745

experiment, the underlying Ir and/or the small portion of the exposed Ir might facilitate the C−H bond activation. The improved methanol oxidation activity of the Pt_xRu_y/Ir/C catalyst in the present experiment, therefore, may represent the combined effects of the ESA (or PtRu utilization), CO tolerance, and enhanced C−H bond activation. However, additional research is needed to verify the role of the underlying Ir. Pt_2Ru_1/Ir/C showed the highest activity among the Pt_xRu_y/Ir/C samples, thus indicating the most efficient surface structure for methanol oxidation. The mass-specific activity of the Pt_2Ru_1/Ir/C sample at 0.5 V was approximately 2.5 times and 1.7 times higher than those of PtRu/C, by considering the PtRu mass and total metal mass, respectively. In the CO stripping study, the ESA of the Pt_2Ru_1/Ir/C sample was 2 times and 1.3 times higher than those of PtRu/C, by considering the PtRu mass and total metal mass, respectively. Therefore, the improvement of methanol oxidation activity is greater than that expected by the enhancement of ESAs, which may be attributed to the combined effect of the CO tolerance and enhanced C−H bond activation. This implies that the positive effect of enhanced C−H bond activation exceeded the negative effect of CO tolerance in the Pt_2Ru_1/Ir/C sample. Chronoamperometry data measured at room temperature shows an activity order which is the same as that of cyclic voltammetry, confirming the results of cyclic voltammetry.

3.3. Single Cell Performance. The single−cell performances of the Pt_2Ru_1/Ir/C and PtRu/C catalysts are compared in Figure 6. The results shows that the DMFC with Pt_2Ru_1/Ir/C

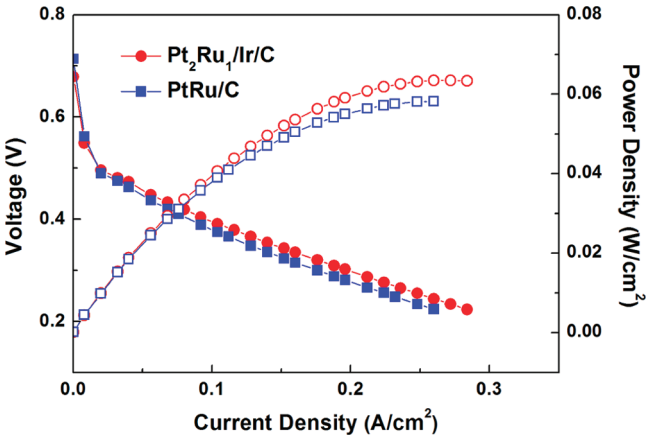

Figure 6. Comparison of single cell measurement results of Pt_2Ru_1/Ir/C and PtRu/C.

as an anode catalyst has a slightly higher cell voltage under the same discharging current density (0.098 and 0.084 A/cm^2 at 0.4 V for the Pt_2Ru_1/Ir/C and PtRu/C catalysts, respectively) and under the maximum power density (0.064 and 0.058 W/cm^2 for the Pt_2Ru_1/Ir/C and PtRu/C catalysts, respectively) despite the fact that the loaded catalyst weight for Pt_2Ru_1/Ir/C is much lower than that for PtRu/C. The anode catalyst loading for Pt_2Ru_1/Ir/C was only 70% in terms of total metal mass and 42% in terms of PtRu mass, as compared with that of PtRu/C. Therefore, the results of the single-cell performance prove that Pt_2Ru_1/Ir/C is a more active catalyst than PtRu/C, and that the synthesis of the PtRu overlayers on Ir nanoparticles can be an effective way to reduce the amount of active materials as the anode catalyst for DMFCs.

4. CONCLUSIONS

PtRu overlayers were deposited on carbon-supported Ir nanoparticles with various overlayer compositions and were applied as catalysts for methanol oxidation. TEM analysis showed that the particle diameters closely corresponded to the calculated values of core−shell structured particles, thus suggesting that the PtRu overlayers were deposited uniformly on the Ir nanoparticles. In addition, the results of EDS point analysis matched well with the experimental conditions. XPS analysis revealed that the fraction of the Ir surface oxides decreased, as a result of core−shell structure formation. Surface characterizations including CV and CO stripping indicated that the exposed Ir surface area was negligible for all Pt_xRu_y/Ir/C samples. The PtRu utilization of the samples was enhanced more than that of PtRu/C because the PtRu atoms or clusters were present only on the surface of particles to form the thin overlayer (or shell) structures. In addition, the C−H bond activation caused by the presence of Ir might have had a positive effect on the methanol oxidation activity. The Pt_2Ru_1/Ir/C sample exhibited the highest mass-specific activity for methanol oxidation, which indicates that it had the surface structure that was most conducive to the electrocatalytic activity of methanol oxidation. The Pt_2Ru_1/Ir/C sample showed slightly higher single−cell performance than PtRu/C, despite the fact that the loaded weight of PtRu in the DMFC that used Pt_2Ru_1−Ir as an anode catalyst was less than half of that of PtRu/C.

■ ASSOCIATED CONTENT

Supporting Information

Deconvolution of XPS data for Pt 4f, Ru $3p_{3/2}$, and Ir 4f signals; chronoamperometry data measured at room temperature in 1 M CH_3OH/0.5 M H_2SO_4 at 0.5 V. This material is available free of charge via the Internet at http://pubs.acs.org.

■ AUTHOR INFORMATION

Corresponding Author

*E-mail: ysung@snu.ac.kr.

Funding

This work was supported by the National Research Foundation of Korea (NRF) (NRF-C1AAA001-2010-0029065) and the Joint Research Project funded by the Korea Research Council of Fundamental Science & Technology (KRCF), Republic of Korea. Y.H.C. acknowledges a financial support by Priority Research Centers Program through NRF funded by MEST (2009-0093814).

Notes

The authors declare no competing financial interest.

■ REFERENCES

(1) Lee, K.-S.; Yoo, S. J.; Ahn, D.; Jeon, T.-Y.; Choi, K.-H.; Park, I.-S.; Sung, Y.-E. *Langmuir* **2011**, *27*, 3128.

(2) Mazumder, V.; Chi, M.; More, K. L.; Sun, S. *J. Am. Chem. Soc.* **2010**, *132*, 7848.

(3) Wang, C.; van der Vliet, D.; More, K. L.; Zaluzec, N. J.; Peng, S.; Sun, S.; Daimon, H.; Wang, G.; Greeley, J.; Pearson, J.; Paulikas, A. P.; Karapetrov, G.; Strmcnik, D.; Markovic, N. M.; Stamenkovic, V. R. *Nano Lett.* **2011**, *11*, 919.

(4) Wang, C.; Chi, M.; Li, D.; Strmcnik, D.; van der Vliet, D.; Wang, G.; Komanicky, V.; Chang, K.-C.; Paulikas, A. P.; Tripkovic, D.; Pearson, J.; More, K. L.; Markovic, N. M.; Stamenkovic, V. R. *J. Am. Chem. Soc.* **2011**, *133*, 14396.

(5) Shao, M.; Shoemaker, K.; Peles, A.; Kaneko, K.; Protsailo, L. *J. Am. Chem. Soc.* **2010**, *132*, 9253.
(6) Wang, D.; Xin, H. L.; Yu, Y.; Wang, H.; Rus, E.; Muller, D. A.; Abruna, H. D. *J. Am. Chem. Soc.* **2010**, *132*, 17664.
(7) Lee, K.-S.; Park, I.-S.; Park, H.-Y.; Jeon, T.-Y.; Cho, Y.-H.; Sung, Y.-E. *J. Electrochem. Soc.* **2009**, *156*, B1150.
(8) Lee, K.-S.; Park, I.-S.; Park, H.-Y.; Jeon, T.-Y.; Sung, Y.-E. *Catal. Today* **2009**, *146*, 20.
(9) Park, I.-S.; Lee, K.-S.; Choi, J.-H.; Park, H.-Y.; Sung, Y.-E. *J. Phys. Chem. C* **2007**, *111*, 19126.
(10) Alayoglu, S.; Nilekar, A. U.; Mavrikakis, M.; Eichhorn, B. *Nat. Mater.* **2008**, *7*, 333.
(11) Sasaki, K.; Naohara, H.; Cai, Y.; Choi, Y. M.; Liu, P.; Vukmirovic, M. B.; Wang, J. X.; Adzic, R. R. *Angew. Chem., Int. Ed.* **2010**, *49*, 8602.
(12) Zhang, J.; Vukmirovic, M.; Sasaki, K.; Neikar, A. U.; Adzic, R. R. *J. Am. Chem. Soc.* **2005**, *127*, 12480.
(13) Sasaki, K.; Wang, J. X.; Balasubramanuan, M.; McBreen, J.; Uribe, F.; Adzic, R. R. *Electrochim. Acta* **2004**, *49*, 3873.
(14) Gong, K.; Su, D.; Adzic, R. R. *J. Am. Chem. Soc.* **2010**, *132*, 14364.
(15) Koenigsmann, C.; Santulli, A. C.; Gong, K.; Vukmirovic, M. B.; Zhou, W.; Sutter, E.; Wong, S. S.; Adzic, R. R. *J. Am. Chem. Soc.* **2011**, *133*, 9783.
(16) Strasser, P.; Koh, S.; Anniyev, T.; Greeley, J.; More, K.; Yu, C.; Liu, Z.; Kaya, S.; Nordlund, D.; Ogasawara, H.; Toney, M. F.; Nilsson, A. *Nat. Chem.* **2010**, *2*, 454.
(17) Yang, R.; Leisch, J.; Strasser, P.; Toney, M. F. *Chem. Mater.* **2010**, *22*, 4712.
(18) Koh, S.; Strasser, P. *J. Am. Chem. Soc.* **2007**, *129*, 12624.
(19) Park, I.-S.; Lee, K.-S.; Jung, D.-S.; Park, H.-Y.; Sung, Y.-E. *Electrochim. Acta* **2007**, *52*, 5599.
(20) Zhao, D.; Xu, B.-Q. *Angew. Chem., Int. Ed.* **2006**, *45*, 4955.
(21) Alexander, W.; Shackelford, J. F. *CRC materials and engineering handbook*, 3rd ed.; CRC Press: Boca Raton, FL, 2001; p 22.
(22) Lee, K.-S.; Jeon, T.-Y.; Yoo, S. J.; Park, I.-S.; Cho, Y.-H.; Kang, S. H.; Choi, K. H.; Sung, Y.-E. *Appl. Catal., B* **2011**, *102*, 334.
(23) Shan, C.-C.; Tsai, D.-S.; Huang, Y.-S.; Jian, S.-H.; Cheng, C.-L. *Chem. Mater.* **2007**, *19*, 424.
(24) Ruban, A.; Hammer, B.; Stoltze, P.; Skriver, H. L.; Norskov, J. K. *J. Mol. Catal. A* **1997**, *115*, 421.
(25) Gurau, B.; Viswanathan, R.; Liu, R.; Lafrentz, T. J.; Ley, K. L.; Smotkin, E. S.; Reddington, E.; Sapienza, A.; Chan, B. C.; Mallouk, T. E.; Sarangapani, S. *J. Phys. Chem. B* **1998**, *102*, 9997.
(26) Eguiluz, K. I. B.; Salazar-Banda, G. R.; Miwa, D.; Machado, S. A. S.; Avaca, L. A. *J. Power Sources* **2008**, *179*, 42.
(27) Geng, D.; Matsuki, D.; Wang, J.; Kawaguchi, T.; Sugimoto, W.; Takasu, Y. *J. Electrochem. Soc.* **2009**, *156*, B397.